Available online at www.sciencedirect.com
SCIENCE DIRECT®
Thermochimica Acta 432 (2005) 158–168
thermochimica acta
www.elsevier.com/locate/tca

Si-N membrane-based microcalorimetry: Heat capacity and thermal conductivity of thin films

B. Revaz [a,*], B.L. Zink [b], F. Hellman [c]

[a] *University of Geneva, Department of Condensed Matter Physics, CH-1211 Geneva 4, Switzerland*
[b] *National Institute of Standards and Technology, 325 Broadway MC 817.03, Boulder, CO 80305, USA*
[c] *Department of Physics, University of California, Berkeley, CA 94720-7300, USA*

Abstract

We have used silicon micromachining techniques to fabricate devices for measuring specific heat or other calorimetric signals from microgram-quantity samples over a temperature range from 1.7 to at least 525 K in magnetic fields to date up to 8 T. The devices are based on a robust silicon-nitride membrane with thin film heaters and thermometers. Different types of thermometers are used for different purposes and in different temperature ranges. These devices are particularly useful for thin film samples (typically 100–400 nm thick at present) deposited directly onto the membrane through a Si micromachined evaporation mask. They have also been used for small bulk samples attached by conducting grease, Ga or In, and for powder samples dissolved in a solvent and dropped onto devices. The measurement technique used (relaxation method) is particularly suited to high field measurements because the thermal conductance can be measured once in zero field and is field independent, while the time constant of the relaxation does not depend on thermometer calibration.

Keywords: Si-N films; Microcalorimetry; Thin films; Thermal conductivity

1. Introduction

In recent years, knowledge of the specific heat and thermal conductivity of small samples has become more important because many materials of scientific and technological interest can be made only in small quantities. Materials such as cuprates, manganites and ruthenates discovered in the last three decades are difficult to synthesize in large, crystalline samples suitable for conventional calorimeters. There are also many materials of current technological and fundamental interest that can only be made in thin film form. These include multilayers, many amorphous materials and magnetic or superconducting systems showing finite size effects. The small mass of such samples typically results in a small heat capacity that is difficult to separate from the background signal of a calorimeter's sample platform, heater and thermometer.

The last 20 years have seen dramatic progress in microcalorimetry, driven primarily by adaptation of technologies developed for the silicon integrated-circuit industry to the design and fabrication of structures with very small length scales. Application of techniques ranging from deposition of metallic and dielectric thin films, photolithographic patterning, anisotropic and deep-trench etching of bulk silicon to e-beam lithography allow the fabrication of reasonably large quantities of repeatable structures of smaller and smaller size with sensitive sensors. These small structures have correspondingly small heat capacities and thermal conductances, allowing fabrication of calorimeters with background heat capacity and thermal conductance small enough to measure thin films and other small samples.

While included at the origin in the parent field of bolometers, microcalorimeters for measurements of small samples have emerged as a separate technique about 10 years ago. In 1994, our group first reported measurements of specific heat of thin films using a Si micromachined microcalorimeter [1]. Since then, microcalorimeters have been developed by many

* Corresponding author. Tel.: +41 22 376 60 78; fax: +41 22 379 68 69.
E-mail address: bermard.revaz@physics.unige.ch (B. Revaz).

0040-6031/$ – see front matter © 2005 Elsevier B.V. All rights reserved.
doi:10.1016/j.tca.2005.04.004

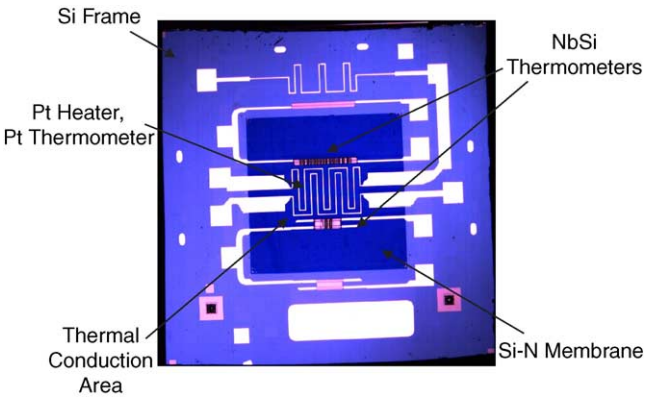

Fig. 1. A top-view of the microcalorimeter. The 10 mm × 10 mm Si frame supports a 5 mm × 5 mm 2000 Å thick a-Si-N membrane. At the center of this membrane, on the back-side, a 2.5 mm × 2.5 mm metal film (not visible in the photo) provides a high thermal conductivity area used to keep the sample, thin film heater and sample thermometers isothermal. The sample (also on the back and not visible) covers this same 2.5 mm × 2.5 mm area (for films) or is attached at the center. The Pt sample heater, and three sample thermometers are visible in the sample area (Pt and two a-Nb-Si thermometers which differ in R and hence useful measurement temperature range due to geometry difference in path width and length); matching thermometers are visible on the Si frame area, which is thermally anchored to a copper block.

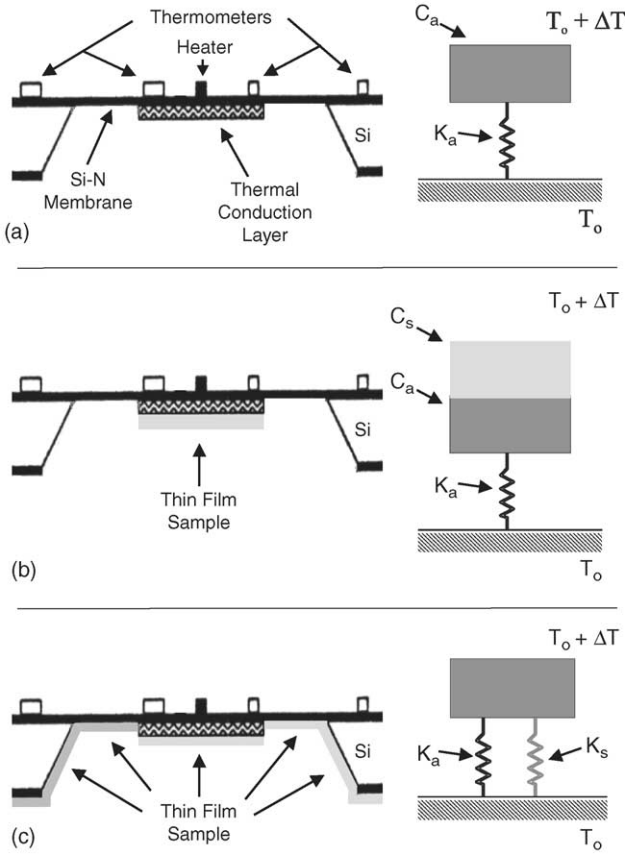

Fig. 2. Side-view schematics of the device with simple thermal models. (a) The microcalorimeter background measurement. (b) To measure the heat capacity of a thin film sample, c_s, a film is deposited on the thermal conduction layer through a micromachined shadow mask. (c) For thermal conductivity measurements a thin film is deposited on the entire block of the membrane, which puts an additional thermal conductance K_s in parallel with K_a.

groups for a wide range of applications in sensor technology, surface science, biology and chemistry. A non-exhaustive list of applications includes thermal conductivity gauges [2], biosensors for monitoring of glucose, urea and penicillin [3], high-throughout thermodynamics measurements for proteomics and drug screening [4]. A remarkable sensitivity has been achieved by Allen and co-workers [5] who report detection of melting in island films of tin using high cooling rate differential scanning calorimeter based on Si-N membranes. A microcalorimeter developed using poly-Si/Al thermopiles sensors by Sarro et al. [6] is now commercially produced by Xensor Integration [7]. These commercial microcalorimeters, together with those produced by PTB Braunschweig, have been studied by Winter and Höhne in a recent paper [8]. Calorimeters made by Xensor have also been used by Schick and co-workers for ultra fast cooling scanning calorimetry of polyethylene samples [9].

A top-view micrograph of a typical device prepared in our laboratory is shown in Fig. 1. The device consists of a ≈2000 Å thick, 5 mm × 5 mm, low-stress a-Si-N membrane supported by a 10 mm × 10 mm crystalline silicon frame. This membrane forms a thermal weak link from a sample deposited or attached to the central area of the membrane to the silicon frame as shown in Fig. 2. Thin film heaters and thermometers patterned on the central area of the membrane allow accurate measurement of the temperature of the sample with respect to the silicon frame when known heating power is applied. Our microcalorimeters have been used for a great variety of measurements, demonstrating a remarkable versatility. We have reported a large number of specific heat studies on thin films [10–15] ($m < 20$ μg) including films grown and measured in situ [16] and films condensed on the membrane from solvent droplets [17], as well as small bulk samples ($m < 1$ mg) [18–21]. The microcalorimeter is useful over a large temperature range (1.7–525 K) and in magnetic fields at least up to 8 T [22]. The same type of device is also planned for measurements in pulsed high magnetic fields. Finally, the functionality of the microcalorimeter has been extended to thermal conductivity measurements [23] as a result of a numerical heat flow analysis [24]. Thermal conductivity of thin films is still not widely available in spite of its importance for many applications. All these results demonstrate that our microcalorimeter is a remarkable platform for microthermal analysis of novel materials.

In this review, we first describe the fabrication and operation of the microcalorimeter. Special attention was given in recent years to the analysis of heat transfer and background contributions of our microcalorimeters. The results of this analysis will be presented as well as the range of samples, which can be measured based on these small backgrounds. We then overview the specific heat and thermal conductivity of the Si-N membrane which is the heart of the

microcalorimeter. Finally, we present a measurement of magnetic multilayer thin films as an example and conclude with a brief consideration of future microcalorimetry techniques and measurements.

2. Microcalorimeter fabrication

Construction of the microcalorimeters begins with a double-side polished (DSP) 4″ (1 0 0) oriented Si wafer. A silicon-dioxide layer is either grown from the wafer using a wet oxidization process at 1000 °C (often called a thermal oxide) or deposited by low-pressure chemical vapor deposition (LPCVD) at 450 °C (commonly referred to as low-temperature oxide, LTO). This underlayer reduces the electrical capacitance between the leads on the completed calorimeter, reducing the noise in the ac resistance measurements of the calorimeter's thermometers. The LTO can be made thicker (1.5 μm), but the thermal oxide is flatter and less porous (thicknesses are 4000–6000 Å). After the oxide is removed from the back of the wafer, we deposit the Si-N layer, which will form the membrane by LPCVD at 835 °C using ammonia (NH_3) and dichlorosilane (SiH_2Cl_2) reagent gases. The film coats the entire wafer surface, front and back. The residual stress is related to the ratio of Si to N in the deposited film, and is controlled by adjusting the NH_3:SiH_2Cl_2 ratio in the furnace during deposition. This stress must be low in order for the film to form a free-standing membrane after the Si substrate is removed from beneath it. Typical compositions for our films are approximately 50% Si and 50% N, which is silicon-rich compared to the stoichiometric compound Si_3N_4 [25,26]. The thickness of the Si-N films is measured with optical interferometry, and is typically between 1800 and 2200 Å. The uniformity in thickness across the surface of a single wafer is normally very good, with deviations ≤20 Å.

After the Si-N layer is deposited, a thin Cr adhesion layer and a 500 Å thick Pt layer are sputtered into the front side of the wafer. Typical base pressures for this deposition are 3×10^{-6} Torr. This layer is photolithographically patterned into bonding pads, leads, thermometers and a heater using 90 °C aqua regia (HCl:HNO_3, 3:1) as an etchant. Use of DSP wafers allows the use of infra-red back-side alignment of square windows in the back-side Si-N to the patterned Pt features. The back-side Si-N is etched using SF_6 plasma. The membranes are then formed by an anisotropic etch in an 80 °C KOH solution. After the Si is removed, a quick dip in HF removes the SiO underlayer, leaving a free-standing Si-N membrane with Pt leads, heater and thermometers in place. For use below 50 K, low-temperature thermometers must also be prepared on the membrane. We use a Cu liftoff procedure to pattern amorphous Nb-Si semiconducting thermometers with two different geometries to span our temperature range. The Nb-Si layer is typically 500 Å and is sputtered from separate targets at base pressures of 5×10^{-6} Torr. The layout of the leads and thermometers is shown in Fig. 1. Fig. 3 shows the resistance as a function of temperature for the three thermometers. Note that each of the three thermometers on the membrane has a matched thermometer on the silicon frame. The paired thermometers form two arms of a resistance bridge.

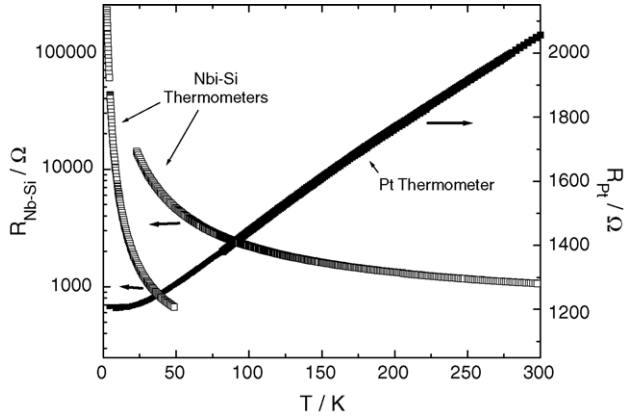

Fig. 3. Example resistances of microcalorimeter thermometers vs. *T*. Note that the a-Nb-Si values are plotted on a log scale (left axis), while the Pt values are plotted on a linear scale.

The final step in fabrication is the deposition of a 2.5 mm × 2.5 mm thermal conduction layer on the center of the membrane, which keeps the heater, thermometers and sample isothermal. This layer is deposited on the back of the membrane through a micromachined shadow mask held within 25 μm of the membrane. Nearly any good metal, such as Au, Ag, Cu or Al can be used as a conduction layer and can be either evaporated or sputtered onto the membrane. This allows some flexibility in the choice of material properties, as well as stress levels in the membrane. This conduction layer in many cases is deposited *after* the deposition of a thin film sample, since the Si-N membrane usually makes a better (flatter and more chemically inert) substrate for sample growth than the metal conduction layer. Note that to ensure isothermal conditions between the thermometer and the sample and to keep the error in the measurement of the specific heat below 2%, the thermal conduction layer generally has to be at least as thick as the Si-N membrane (typically 2000 Å). Because the geometry of the calorimeter is known or can be measured with high accuracy, we can construct a numerical model of the 2D heat flow in the calorimeter [24]. Key results from this simulation appear in the description below.

3. Experimental technique

The microcalorimeter is clamped to the copper sample stage of a cryostat and wires are ultrasonically bonded to the calorimeter's heaters and thermometers. The microcalorimeters have been used in a wide range of cryostats including simple LHe and LN_2 systems, a cryostat with a cold finger that extends into a UHV deposition system for in situ studies, and high field magnet systems ranging from standard

superconducting solenoids to high field magnets at NHMFL (currently under development). In all cases, the area around the calorimeter is pumped to high vacuum ($<1 \times 10^{-7}$ Torr) and this vacuum is maintained throughout the measurement. The vacuum around the calorimeter is important both because of the need for low thermal conductance to the environment (including parts which are at not at the temperature of the Cu sample stage) and because small amounts of gas or ice on or around the membrane unpredictably and irreproducibly alter the background contributions. The temperature of the copper block is typically monitored with a calibrated temperature sensor and temperature controller and the sequence of measurements performed and recorded through GPIB connections by a PC running Labview.

For most specific heat measurements we use the small ΔT relaxation method. This technique is well known as the best compromise when precise and absolute values of the specific heat of small samples are desired over a large temperature range [27]. However, this technique is not ideal for the study of sharp phase transitions, such as the magnetic phase transitions of small crystals of $SrRuO_3$ [18] and $La_{1-x}Ca_xMnO_3$ [19], due to the limited temperature resolution and the large number of steps that are required. For these measurements, we have used the so-called large ΔT relaxation technique (a version of the sweep method) [19,27].

Measurements of specific heat using the small ΔT relaxation method in the membrane based configuration requires the thermal conductivity and the specific heat (per unit of surface) of the sample to be large with respect to those of the membrane. This point will be discussed in more details below. When these conditions are fulfilled, the specific heat can be obtained by measuring two quantities: the thermal conductance, K_a, and the time constant, τ, of the sample's relaxation to the temperature of the bath. Though the techniques used to fabricate these calorimeters result in very small deviations in properties, including c_a and K_a, from one device to another, the resistances of the thermometers do vary from one microcalorimeter to the next. Each measurement therefore also includes a calibration of the device's thermometers against a calibrated Cernox thermometer located in the regulated copper block.

To measure the time constant, τ, of the relaxation, we first apply a small current to the sample heater (typically chosen to give $\Delta T/T \approx 0.01$) and wait for thermal equilibrium. We then set the heater current to zero and record the response of the sample thermometer as it cools to the temperature of the bath. As long as the thermal link between the sample and the thermometer is large compared to K_a (so that the sample and thermometer remain essentially in thermal equilibrium), and for sufficiently small heating power, this relaxation follows a single exponential curve. Fitting this measured curve gives the value of the time constant, τ. For the addenda measurement (and for some samples with low heat capacity at low T), τ becomes short at low T. In this circumstance, the ac resistance bridge [28] must be driven with a high enough frequency to avoid losing information in the short fall time of the decay. Typically, we find a frequency of several hundred Hz is needed to measure the $\approx$10 ms τ of the addenda at 2 K.

The first step in measuring either heat capacity or thermal conductivity of a sample is measurement of the background resulting from elements of the calorimeter other than the sample films. For C_P measurements this background is the addenda heat capacity c_a and for k measurements the background is the thermal conductance of the link between the central heated area (defined by the thermal conduction layer) and the bath, K_a. In a typical specific heat measurement, the sample space of the bare microcalorimeter is first covered with a thermal conduction layer (Al, Cu or Au) of typically 200 nm. The specific heat of this microcalorimeter is then measured and fitted as a function of temperature, which gives the background specific heat c_a called "addenda". The thin film sample is then deposited on top of the conduction layer and the microcalorimeter specific heat c_{tot} is measured again. The specific heat of the sample c_s is finally obtained by a simple subtraction $c_s = c_{tot} - c_a$ and proper volume or mass normalization. Simple side-view schematics and thermal models for the microcalorimeter describing the contributions to the specific heat or thermal conductivity are shown in Fig. 2. These contributions will be discussed in details below. Note that the thermometers located on the microcalorimeter are separately calibrated for each measurement, so that possible variations of the properties of the sensors caused by the deposition of the sample do not affect the measurement.

The error Δc due to the temperature variation of the specific heat across the interval ΔT is usually negligible. It can be estimated assuming that Δc is the difference between the value $c(T + \Delta T/2)$ and the measured value $\langle c \rangle = (\int_T^{T+\Delta T} c(T)\,dT)/\Delta T$ which is a mean over the interval ΔT. Using a power low approximation for the specific heat $c(T) = AT^n$, gives $\Delta c/c = (n(n-1)/24)(\Delta T/T)^2$. For materials measured at temperatures far from phase transitions, this exponent n is typically less than 3, so that taking a temperature interval of 2% would result in a negligible error <0.01% on the specific heat.

To measure K_a, the temperature of the microcalorimeter is stabilized at T_0 and the ac resistance bridge is balanced. A small amount of heating power, P, is applied to the center of the membrane by causing a known current to flow in the sample heater. A concurrent measurement of the voltage drop across the heater gives the measured heating power P. When thermal equilibrium is reached, to good approximation (discussed further below) the thermal conduction layer, heater and thermometers are isothermal at $T_0 + \Delta T$. The change in resistance, ΔR, of the membrane thermometer relative to the matched thermometer on the silicon frame is detected as an off-null signal by a lock-in amplifier and ΔR converted to ΔT using the thermometer calibration. Because this measurement is essentially steady-state, the ac resistance bridge is driven at a relatively low frequency (often $\approx$17 Hz) to avoid signal attenuation which occurs at higher frequencies. The heating power is related to the steady-state ΔT by $P = \langle K_a(T, T_0) \rangle\, \Delta T$. Here, $\langle K_a(T, T_0) \rangle$ is the average thermal conductance of the

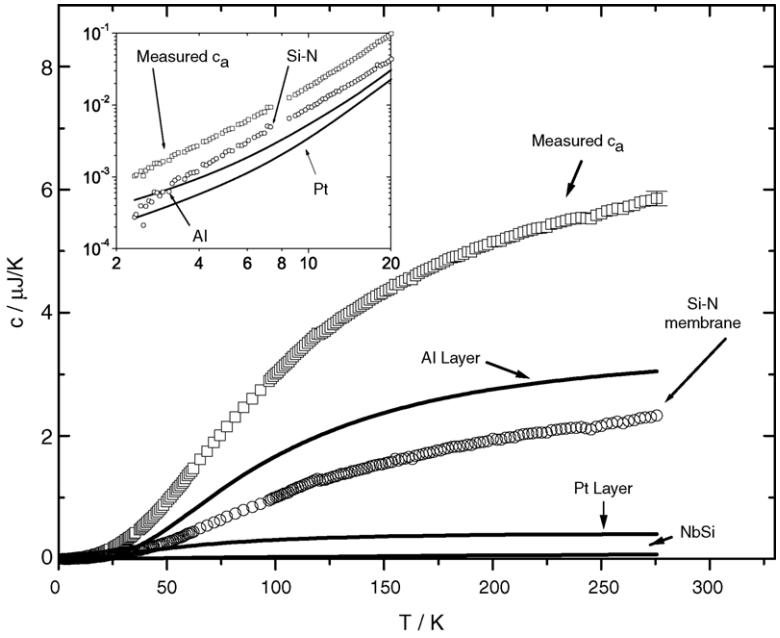

Fig. 4. The addenda heat capacity c_a, with the contributions from elements of the microcalorimeters. The error on the measurements is ≈2% (form Ref. [23]).

link over the temperature range T_0, $T_0 + \Delta T$. $K_a(T)$ is determined from this average with a two-variable fit. In practice, we find that K_a is close to linear over the small values of ΔT (typically 1–10% of T_0) and we replace the average $\langle K_a(T, T_0)\rangle \approx K_a(T_0 + \Delta T/2)$, again giving the thermal conductance as a function of a single temperature. As a consistency check, at each T_0 we typically measure ΔT for a series of increasing applied P. The heat capacity is given by $c = K_a\tau$.

The addenda specific heat, c_a, for this microcalorimeter is the result of contributions from the Si-N membrane, the thermal conduction layer, the Pt leads, heater and thermometer and the Nb-Si thermometers. An example is shown in Fig. 4. The dominant contribution for most temperatures is the metallic conduction layer (an Al layer for this calorimeter). The inset shows the same plot at low temperatures. The heat capacity of the Nb-Si is approximately an order of magnitude smaller than that of the metal layers and is not shown in the inset. The area of each of the features contributing to c_a is precisely known from the photolithography; the thickness is determined either by profilometry or inferred from growth parameters and comparison to other devices. We used literature values for C of Al, Cu and Pt [29,30] and approximated the specific heat of a-Nb-Si with a similar composition of a-Y_x-Si_{1-x} [31]. Calculating the contribution of the conduction layer, Pt heater and thermometer, and the a-Nb-Si thermometers is straightforward, as these features are isothermal to good accuracy. The contributions of the Pt leads and Si-N membrane are more complicated, as a thermal gradient exists across these features. In the 1D case, Bachmann et al. showed that 33% of the heat capacity of the heat link had to be included in the addenda [32]. 2D heat flow simulations [24] indicate that under typical conditions, 24% of the Si-N membrane outside the sample area contributes to c_a. The Pt leads contribution obtained using the same calculations is 33% as expected for 1D heat links (see Fig. 1). The contributions of the Pt and a-Nb-Si features are small compared to the membrane and thermal conduction layer, and any error from deviations of the real material's specific heat from literature values is therefore negligible.

The heat capacity of Si-N (in J/K) shown in Fig. 4 was determined from c_a by subtracting the Pt, Al and a-Nb-Si contributions. This can be converted to $C_{Si\text{-}N}$ (in J/g K) using the geometry of the Si-N ((2.5 mm × 2.5 mm central sample area + 0.24((5 × 5) − (2.5 × 2.5)) mm^2 border area) and a typical density $\rho = 2.865\ g/cm^2$. Measurements using different metals for the conduction layer (Al, Cu, Au) give the same values of C for Si-N, giving confidence that the deviation from the literature values of these metals is small.

Fig. 5 shows the thermal link of the microcalorimeter, K_a, which consists of only two contributions, from the Pt leads and Si-N membrane. However, above 100 K heat losses from radiation must be subtracted (a procedure described elsewhere [33,34]). The contribution of the Pt, K_{Pt}, is determined from the Wiedemann–Franz law ($k/\sigma = L_0T$), where σ is the electrical conductivity, determined for each calorimeter by measuring the resistance of the Pt heater. Correcting for radiation and subtracting K_{Pt} gives $K_{Si\text{-}N}$ and, as for a deposited sample film, the thermal conductivity can be calculated from $k_{Si\text{-}N} = K_{Si\text{-}N}/\alpha t$, where t is the film thickness determined by optical interferometry.

After c_a is measured we deposit a thin film sample onto the conduction layer at the center of the membrane, using a shadow mask held within 25 μm of the membrane to define the sample area. This limits shadowing effects due to multi-element deposition or sputtering deposition to 1% for a 0.25 cm × 0.25 cm sample. Since it is often preferable to

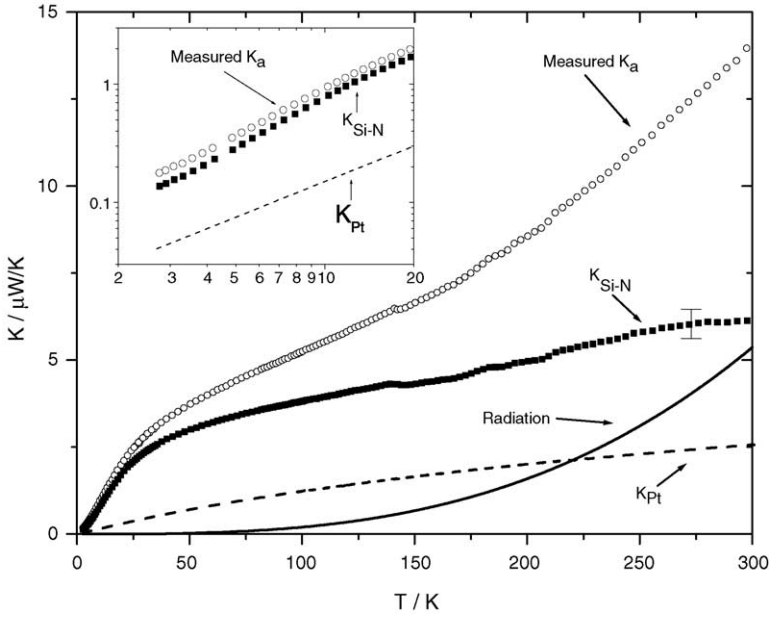

Fig. 5. The measured thermal link, K_a, of the microcalorimeter (open circles) shown with the contributions from radiation and from the elements of the device. The contribution of the Pt leads is determined by measuring the resistivity of the Pt and calculating k_{Pt} using the Wiedemann–Franz law. The radiation contribution is given by $4\sigma\varepsilon AT^3$ [33]. The contribution of the Si-N membrane is the result of subtracting these contributions from K_a. The high T error is determined by the uncertainty in the radiation term. Below 100 K, the error is ≈5% (from Ref. [23]).

grow a film directly on the very flat Si-N membrane surface, rather than on the metallic conduction layer, for some studies we measure a sample with the conduction layer deposited on top, and determine c_a by measuring a device from the same wafer with a conduction layer only; the thermal link and the specific heat of the addenda typically vary by less than 5% within a wafer [34].

Bulk samples are attached on the thermal conduction layer with In [18,19] or Ga [35]. While greases of various kinds have been successfully used for low temperature measurements, care must be taken when measurements at moderate temperature (77–300 K) are desired as the grease undergoes a glass transition in that regime which has been observed to lead to irreproducible heat capacity, which depends on cooling rate and history [36].

As shown in Fig. 2b the heat capacity of the sample c_s is added to the addenda heat capacity c_a, increasing τ while leaving K_a constant. In first approximation, c_s can then be determined simply by subtracting c_a from $K_a\tau = c_a + c_s$ and the specific heat of the sample C may then be calculated from c_s using the sample volume and either its molar volume, giving C in J/mol K, or its mass density, giving C in J/g K. There are two main effects which can introduce systematic errors when this simple subtraction is used. First, the fraction of the membrane that contributes to c_a depends on the ratios c_{2Ds}/c_{2Dm} and k_{2Ds}/k_{2Dm}. Here, c_{2Dm} is the specific heat per unit surface (J/K cm^2) of the membrane and c_{2Ds} is the specific heat per unit surface of the combined thin film sample and conduction layer. Similarly, k_{2Dm} is the thermal conductivity multiplied by the thickness of the membrane (giving units of W/K) and k_{2Ds} is the same quantity for the combined conduction layer and sample film. The second effect that can introduce systematic error when using the simple difference method are deviations from a single time constant relaxation which occur for low c_{2Ds}/c_{2Dm} or low k_{2Ds}/k_{2Dm} values. Because values for c_{2Ds}/c_{2Dm} and k_{2Ds}/k_{2Dm} can vary over five orders of magnitude depending on the samples and temperature, and because the contributions of the membrane and the Pt leads to K_a vary differently as a function of temperature, a detailed analysis of the heat transfer in Si-N membrane-based calorimeters with thin film samples is necessary to provide a firm understanding of these potential systematic errors. The results of this finite element analysis study are reported in a recent paper [24]. Note that these issues have no equivalent in a bulk calorimeter, with the exception of the variation of the contribution of the thermal link to the addenda heat capacity as a function of the thermal load.

In these calculations, we assumed a 2D heat transfer, which is justified by the small thickness of the components (sensors, membrane, leads, sample) of the microcalorimeter with respect to the lateral dimensions. As a consequence, the temperature along the direction perpendicular to the microcalorimeter plane can be considered as constant at any time. At low temperature this assumption would need to be reconsidered due to Kapitza thermal boundary resistance and possible changes in surface scattering once the phonon mean free path exceeds the membrane thickness (see below); we note however that since both sample and thermometer are films grown directly on the membrane, this acoustic mismatch issue may be not relevant. The contribution of the thermal link, the deviation from the single time constant decay, and the error made using the $K_a\tau = c_a + c_s$ approximation,

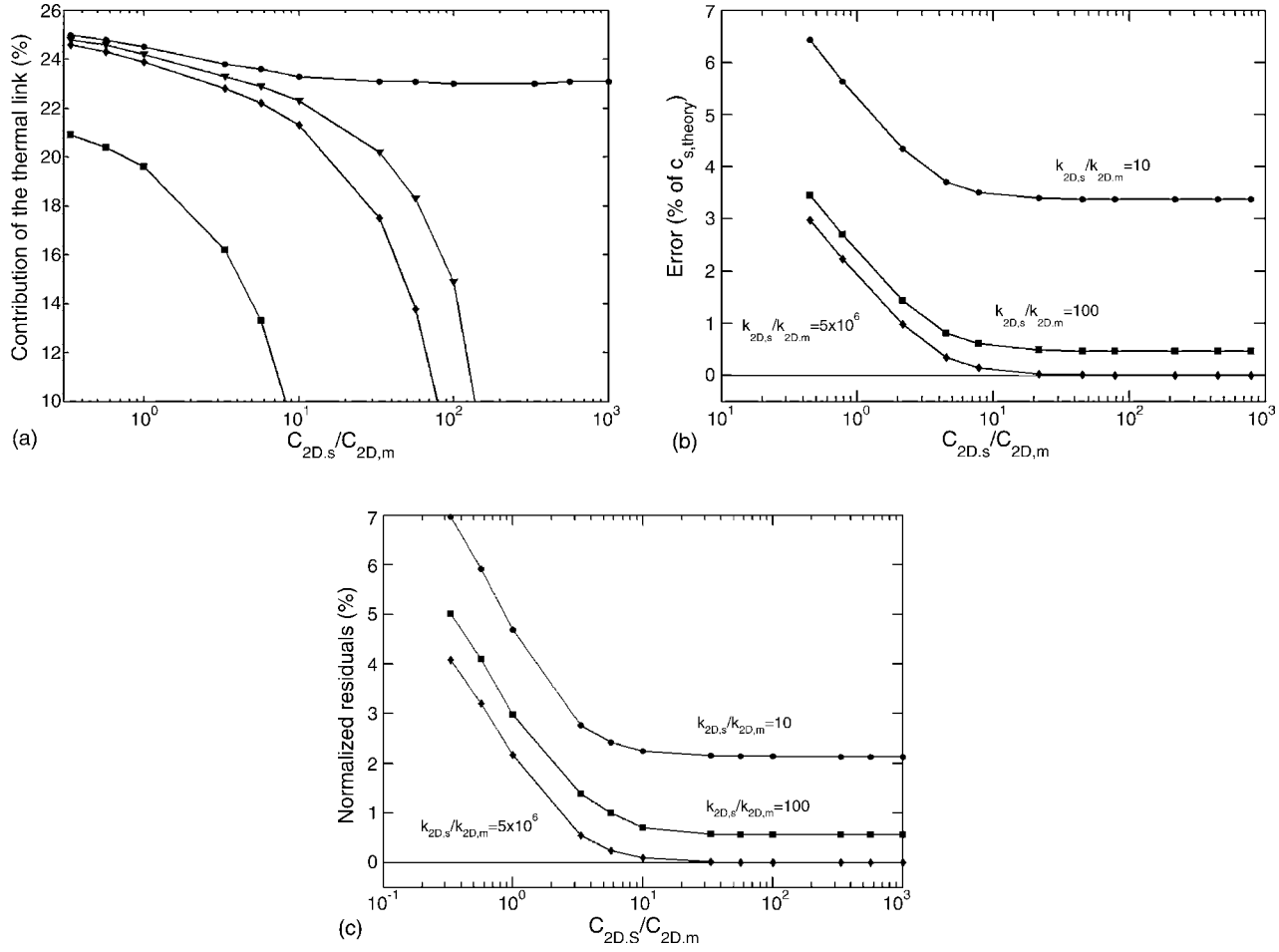

Fig. 6. (a) Contribution of the thermal link to the total specific heat for various values of k_{2Ds}/k_{2Dm} (5×10^6, 200, 100 and 10 from top to bottom). (b) Error on the specific heat of the sample obtained by the simple subtraction $K_a\tau = c_s + c_a$ (see text) for various values of k_{2Ds}/k_{2Dm}; c: normalized residues of single time constant decay fits of the numerical data for various values of k_{2Ds}/k_{2Dm} (from Ref. [24]).

calculated for various values of c_{2Ds}/c_{2Dm} and k_{2Ds}/k_{2Dm}, are reported in Fig. 6a–c. From these results, we conclude that this simple approximation gives an error of $\leq$2% in the common range of c_{2Ds}/c_{2Dm} and k_{2Ds}/k_{2Dm} values used with our calorimeters. The small systematic error can be taken into account in the calculation of c_s. It is important to note that low k_{2Ds}/k_{2Dm} values do not lead to strong, visible deviations of the relaxation with respect to a single time constant decay (contrary to the so-called τ_2 effect due to bad thermal coupling between a bulk sample and the calorimeter) but nonetheless strongly increase the error on the sample specific heat calculated in the single time constant approximation when $k_{2Ds}/k_{2Dm} < 5$.

To measure thermal conductivity of a thin film sample, first K_a is measured as described above. As shown in Fig. 2c, a thin film sample is then deposited on the entire back of the membrane. This adds a contribution K_s in parallel to K_a so that $P/\Delta T = K_a + K_s$. K_s is then determined by subtracting K_a from the total thermal conductance measured after sample deposition. The sample thermal conductivity is then given by $k = K_s/\alpha t$, where α is a 2D geometry factor and t is the sample film thickness. When the central heater/thermometer area is isothermal, $\alpha = 10.33$ [24]. Deviations from this behavior based on calculations of heat flow in the 2D membrane are discussed in detail elsewhere [24]. Above 100 K, where radiation contributions become significant and may change with the addition of the sample, and below 10 K, where the phonon mean free path in the membrane becomes comparable to membrane thickness, hence surface scattering affects thermal transport in the membrane and can be altered by addition of the sample, K_s may not be determined by this simple subtraction. These more complicated cases are discussed in detail elsewhere [34,34].

4. Measurements in high magnetic fields

These microcalorimeters together with the relaxation method are ideally suited for measurement of specific heat in a field due to their compact self-contained nature and the lack of dependence of the background contributions on field. Systematic measurements of the magnetic field dependence

of the microcalorimeter indicate no magnetic field dependence in K_a or c_a down to $T = 2$ K in fields up to at least 8 T [22]. The field-induced change in the a-Nb-Si resistance has been found to be less than 1% above 12 K. At lower temperatures, a negative magnetoresistance is observed between 0 and 4 T while higher magnetic fields increase the resistance of the thermometer. Even in this temperature range, the overall magnetoresistance is found to be less than 2%.

In preparation for use of these devices to still higher fields, magnetoresistance measurements were performed at the National High Magnetic Field Lab (NHMFL) on both Pt and a-Nb-Si in fields to 32 T down to 1.3 K. For sensors with R (4.2 K) between 2 and 10 kΩ, the magnetoresistance at this temperature shows a tendency towards saturation around 32 T, with $\Delta R/R$ reaching 35–40% at this field. These values are similar for various field and current orientations. At 69.5 K, the magnetoresistance of NbSi is negligible, reaching a plateau around 8 T ($\Delta R/R \sim 0.06\%$), and slightly decreasing above 17 T. Measurements on Pt thermometers were made with the field parallel and perpendicular to the plane of the film, with current perpendicular to the field in both cases. $\Delta R/R$ at 3 and 4.2 K is 0.15–0.2% at 32 T. These measurements suggest that the microcalorimeters are a solution for specific heat measurements in magnetic field up to at least 32 T. For proposed use below 1 K, the contribution of the Pt leads to the thermal conductance K_a is calculated to become dominant, hence its possible field dependence would be important to determine before relying on the field independence of K_a. This is readily determined through the electrical conductivity via Wiedemann–Franz, which should apply well in this limit.

It is important to point out that the magnetoresistance of the *device* thermometers has little direct effect on the functionality of the devices even in high fields, as long as the temperature sensitivity remains large. This is because in the heat–capacity relaxation technique the time constant measurement does not require that the thermometers be calibrated, while thermometer calibrations and thermal-link conductance measurements will be performed in zero field. Magnetoresistance of the *block* thermometers, which provide the temperature for the measurement T_0, must be determined separately, as for any measurement in high field.

5. Estimate of uncertainty: range of possible samples

Because the active elements of the microcalorimeter are all thin films, the background heat capacity (shown in Fig. 4) and the background thermal conductance K_a (Fig. 5) remain small. This allows accurate measurements of the heat capacity of thin films or small bulk samples and the thermal conductivity of thin films. Fig. 7 illustrates this point for the heat capacity measurement. The plot is of sample heat capacity c_s versus T. Solid lines show the value of c_s required at each T for the expected uncertainty in c_s to be ≈1.5, 2, 5, 10 and 20%. This calculation assumes that the conduction layer,

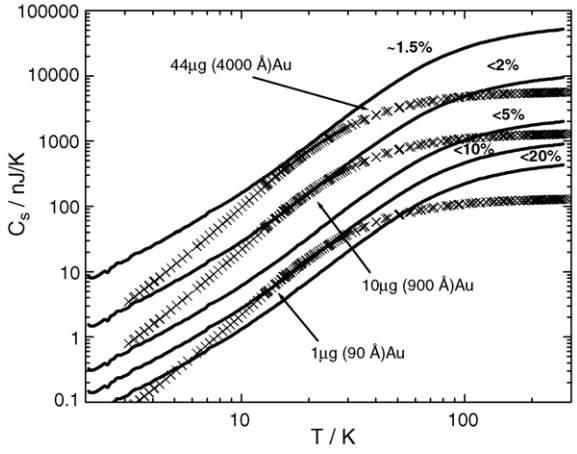

Fig. 7. Plot of sample heat capacity c_s vs. T. The solid lines indicate values required for estimated relative error on c_s to be 1.5, 2, 5, 10 and 20%. X's are calculated for stated mass (thickness) of a Au film, assuming the literature C_P values [29,30].

heater, thermometers and sample are essentially isothermal and that the uncertainties in measurement of τ and K_a are 1%. X's show the heat capacity of Au samples of various mass (thickness) based on literature values of the specific heat of Au [29,30]. For a 44 μg (4000 Å) thick Au film, we expect <3% error at all T, while for a 1 μg (90 Å thick) film we expect better than 20% uncertainty below 50 K.

A similar plot for the thermal conductivity measurement appears in Fig. 8. Here, we plot the product of sample thermal conductivity and thickness, $k_s t$, versus T. Solid lines show required values of $k_s t$ for the expected uncertainty in k_s to be ≈0.03, 0.05, 0.10 and 0.20. The dashed lines shown above 100 K and below 10 K are the radiation and surface scattering regions where the estimation of error depends on sample emissivity and surface properties of both the sample and

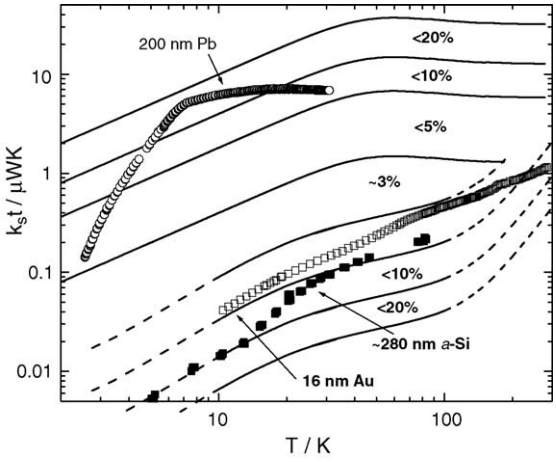

Fig. 8. Plot of the product of sample film thickness and sample thermal conductivity, $k_s t$, vs. T. Solid contour lines show required values for estimated relative error on k_s to be 3, 5, 10 and 20%. Dashed lines indicate conditions where estimate of error depends on details of the microcalorimeter or sample due to surface scattering (low T, low $k_s t$) or sample emissivity ($T > 100$ K). Symbols indicate measured values for Pb and Au [33] and a-Si [48] films.

the nitride membrane as described in detail elsewhere [33]. Below 100 K the lower $k_s t$ contour lines are set by the 1% uncertainty in measurement of K_a, and $K_a + K_s$ and a 2% uncertainty in t.

The upper $k_s t$ limits are set by the requirement for maintaining thermal equilibrium in the central heater and thermometer area. As mentioned above, $\alpha = 10.33$ holds while the temperature gradient is confined to the area between the central conduction layer and the Si frame. As k_s or t for the sample film increases (relative to kt for the conduction layer), the temperature gradient across the conduction layer grows and α is reduced, leading to systematic underestimation of k_s, which is calculated in Ref. [24]. Measured values of $k_s t$ for a 200 nm Pb film, a 16.3 nm Au film and a 277 nm a-Si film are also plotted in Fig. 8.

6. Specific heat and thermal conductivity of the amorphous Si-N membrane

Disordered solids such as the low-stress amorphous Si-N which forms the microcalorimeter membrane typically have low thermal conductivity, k, compared to crystals, with a plateau generally around 10–50 K above which k continues to increase with temperature, similar temperature dependence and magnitude below ≈10 K, and $k \propto T^{1.8}$ below 1 K [37–40]. In the specific heat of these materials, two features are nearly universally observed. The first is a linear term at $T < 1$ K due to a constant density of the two-level state systems (TLS) which also dominate phonon scattering and lead to the characteristic low T behavior of k [37,40]. The second is a broad peak or bump in C/T^3 versus T, which occurs at the same temperature as the plateau in k. The height of this peak, P_c, also typically scales with the temperature at which it occurs, T_{max}, so that $P_c \propto {T_{max}}^{-1.633}$. This bump and the corresponding plateau in k indicate a large density of relatively low-energy vibrational states, but the physical origin of the scaling behavior is not yet understood.

Fig. 9a compares our experimental results for $C_{Si\text{-}N}$ (grown on LTO or on thermal oxide) to vitreous silica (SiO_2) on a log–log C/T^3 versus T plot. The peak around 10 K seen in SiO_2 is the characteristic peak seen in amorphous solids [41], while the low temperature upturn is due to the linear term associated with two-level tunneling systems. The solid line is the Debye function for crystalline Si_3N_4 ($\Theta_D = 1130$ K) [42]. The Debye specific heat is constant below $\Theta_D/10$ on this type of plot, and decreases at high T. The short dotted line near the y-axis indicates the low temperature value of a Debye specific heat calculated for a-Si-N using the measured sound velocity in similar membranes [43,44]. The small arrow indicates the location of the expected peak in C/T^3 for Si-N in C/T^3 [23]. C/T^3 for Si-N grown on thermal oxide continues to increase down to 3 K, indicating non-T^3 behavior similar to that seen in other amorphous materials at lower T (due to TLS).

Fig. 9b compares our measured thermal conductivity $k_{Si\text{-}N}$ to amorphous Si-N films grown by LPCVD (LP1 [45], LP2 [43]), PECVD (PE [46]) and APCVD (AP [46]), as well as vitreous silica [38]. Our results agree well with other measurements of LPCVD Si-N. The difference in k between the LPCVD films and those grown by plasma enhanced CVD (PECVD) or atmospheric pressure CVD (APCVD)[46] is likely to be a result of different film microstructures. All measurements of LPCVD Si-N indicate a very large k at high temperatures for an amorphous solid. The shape of the curve is typical, with a plateau beginning at ≈20 K but extending to a relatively high ≈100 K; the same temperature range where the weak maximum in C/T^3 is indicated in Fig. 9a as expected. The low temperature, $k_{Si\text{-}N}$ values are within the range of previously measured amorphous solids [39]. The inset in Fig. 9b shows our estimation of the phonon mean free path, ℓ, in our Si-N membranes below 20 K on a log–log plot [23]. This is shown for two membranes, one grown on a thermal oxide underlayer and one grown on a LTO underlayer.

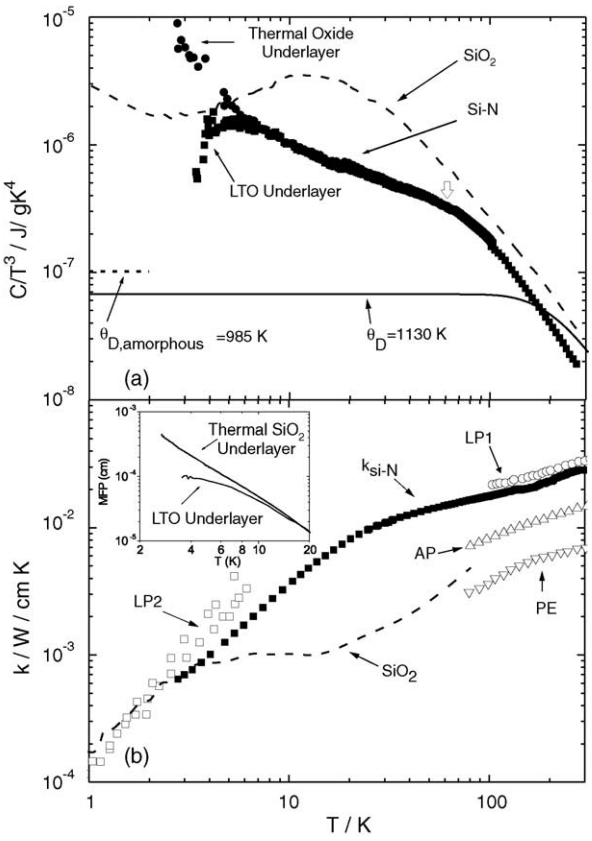

Fig. 9. (a) C/T^3 vs. T on a log–log plot comparing our measurements of Si-N ((■) LTO underlayer, (●) thermal oxide underlayer) with vitreous silica [38], and a Debye function with the $\Theta_D = 1130$ K literature value for bulk Si_3N_4 [42]. The short dotted line is the low T limit of C/T^3 using Θ_D, amorphous, calculated from the sound velocity in a-Si-N. The open arrow indicates the likely location of the C/T^3 peak for Si-N. (b) $k_{Si\text{-}N}$ of a film grown on thermal oxide (■, labeled $k_{Si\text{-}N}$) compared to values reported by other groups. *Inset:* Phonon mean free path ℓ below 20 K vs. T on a log–log plot. Value are calculated from our measured k for two microcalorimeters and C_{Debye} using $k = 1/3 C_{Debye} v \ell$, where v is the measured sound velocity in similar membranes [43] (from Ref. [23]).

At high T ($T > 100$ K not visible on this plot) all curves approach the inter-atomic spacing (~2.5 Å for Si-N), and increase rapidly as the temperature decreases. Below 20 K, ℓ for both membranes exceeds the 2000 Å membrane thickness. The two different membranes differ below this point. ℓ continues to increase for the membrane grown on the thermal oxide underlayer, while ℓ in the membrane grown on LTO is reduced and appears to reach a limiting value of 1 μm. This behavior indicates that diffuse surface scattering dominates the phonon transport in the Si-N grown on LTO. Phonons incident on the rough surface are scattered in all directions with equal probability. Values of ℓ seen in the Si-N grown on thermal oxide which exceed the membrane thickness indicate that specular scattering occurs at the surfaces. This is likely due to the different bottom surface created by growing on different oxides. We expect that when Si-N is grown on the flatter thermal oxide, a smoother surface is left behind when the oxide is etched away. Scattering off this smoother surface would be at least partially specular, while scattering off the rougher surface left after removal of the LTO would cause more diffuse scattering, reducing ℓ in the temperature range below 20 K where the intrinsic ℓ exceeds the membrane thickness.

These surface scattering effects introduce a complication for measuring k of thin films at low T with this microcalorimeter. Previous studies show that thin films deposited on very clean surfaces of pure Si wafers can disturb specular surface scattering, causing reduction of the mean free path and thermal conductivity [47]. There is some indication that similar physics occurs in thicker a-Si-N membranes [43]. If the phonon scattering at the bottom membrane surface is predominantly specular, deposition of the sample film on this surface causes the scattering to be partially diffuse, changing the thermal conductivity of the membrane. In this case, $K_s \neq P/\Delta T - K_a$. We present a more complete description of these effects elsewhere [23].

7. Specific heat measurements of thin films and single crystals

Samples measured to date include amorphous magnetic films (a-TbFe2 and giant negative magnetoresistance a-Gd-Si alloys) [12,13], empty and filled fullerenes (C60, K3C60, C82, La@C82, C84, Sc2@C84) [16,17], single crystal and pressed pellets of manganites and ruthenates [18–20], magnetic and antiferromagnetic multilayered films (Fe/Cr; NiO/CoO, NiO/MgO and CoO/MgO; CoO/SiO2) [10,11,15].

Specific heat studies of magnetic materials are useful in several ways: characterization of the nature of the magnetic transition, determination of the magnetic entropy evolved and hence the number of magnetic states populated between $T = 0$ and the transition and/or above the transition, and characterization of the low-energy magnetic excitations of the system. Specific heat measurements allow a characterization of the magnetic transition and low-temperature properties in zero magnetic field, a useful property when magnetic measurements may be complicated by magnetic history dependence such as in spin glasses. They also reflect the bulk thermodynamic properties, and hence are particularly valuable when magnetic measurements may be dominated by impurity phases or surface effects as in antiferromagnets and superconductors.

An important application of these microcalorimeters is measuring specific heat of magnetic multilayers (MML) with giant magnetoresistance (GMR), which are heterostructures of great technological significance. These MML consist of alternating ferromagnetic (i.e. Fe, Co) and non-magnetic (i.e. Cu, Cr, Ag) layers, where the magnetic layers are coupled in an antiparallel configuration in zero applied magnetic field. We deposited a Fe/Cr MML on the microcalorimeter and compared the measured specific heat with that of pure Fe and Cr thin film samples. The thickness of all samples was around 1000 Å. In this study, we especially concentrated on the low temperature electronic contribution to the specific heat, from which the electronic density of states, γ, can be determined. γ is an important parameter for itinerant ferromagnets, and particularly important for understanding the electronic transport which determines GMR. We observed that at low temperature, γ is strongly enhanced in the Fe/Cr sample with respect to the pure Fe and Cr samples but is independent of magnetic field, hence not directly *leading* to GMR (but still necessary for *understanding* GMR). We also observed a softening of the phonon modes, which may be in part responsible for the enhancement of the electronic contribution. This study is described in detail in Ref. [15].

8. Conclusion

In this article, we have reviewed our techniques for measuring specific heat of thin films and small bulk samples and thermal conductivity of thin films. Though there is a great deal of science still to be discovered using our current capabilities, we are also working to extend Si-N membrane-based microcalorimetry techniques to lower temperatures (0.3 K) and pulsed magnetic fields up to and beyond 32 T. We are also developing microcalorimeters with thinner membranes (30 nm) to allow measurement of yet smaller heat capacities and thermal conductivities and exploring the use of surface micromachining to integrate the shadow mask and microcalorimeter to simplify sample preparation and further reduce systematic uncertainties.

Acknowledgements

We would like to thank the DOE and NSF for support and all the members of the Hellman group for their contributions to the development of this technique: D.W. Denlinger, E.N. Abarra, K. Allen, P.W. Rooney, M.T. Messer, S.K. Watson, D.K. Kim, S. Wohlert, E. Janod, R. Sappey, D. Lieberman,

A. Kuprin, Y.-J. Tang, D. Queen, D. Cooke, as well as the National High Magnetic Field Lab and the Berkeley Microlab and faculty and students there who have helped us over the years. One of us (B.R.) thanks the Swiss National Fund and the Swiss National Center for Competence in Research MaNEP for financial support.

References

[1] D.W. Denlinger, E.N. Abarra, K. Allen, P.W. Rooney, S.K. Watson, F. Hellman, Rev. Sci. Instrum. 65 (1994) 946.
[2] http://www.xensor.nl/pdffiles/sheets/tcg3880.pdf.
[3] F. Bataillard, E. Steffgen, S. Maemmerli, A. Manz, H.M. Widmer, Biosen. Bioelectron. 8 (1993) 89.
[4] F. Raymond Salemme, Nat. Biotechnol. 22 (2004) 1100.
[5] S.L. Lai, J.Y. Guo, V. Petrova, G. Ramanath, L.H. Allen, Phys. Rev. Lett. 77 (1996) 99.
[6] P.M. Sarro, A.W. van Herwasrden, W. van der Vlist, Sens. Actuators A 41–42 (1994) 666.
[7] For more information see http://www.xensor.nl/.
[8] W. Winter, G.W.H. Höhne, Thermochim. Acta 403 (2003) 43.
[9] S.A. Adamovsky, A.A. Minakov, C. Schick, Thermochim. Acta 403 (2003) 55.
[10] Y.J. Tang, et al., Phys. Rev. B 67 (2003) 054408.
[11] E.N. Abarra, K. Takano, F. Hellman, A.E. Berkowitz, J. Appl. Phys. 79 (1996) 5919.
[12] B.L. Zink, et al., Phys. Rev. Lett. 83 (1999) 2266.
[13] F. Hellman, et al., Phys. Rev. B 58 (1998) 5672.
[14] E.N. Abarra, et al., Phys. Rev. Lett. 77 (1996) 3451.
[15] B. Revaz, et al., Phys. Rev. B 65 (2002) 94417.
[16] K. Allen, F. Hellman, Phys. Rev. B 60 (1999) R11765.
[17] K. Allen, F. Hellman, J. Chem. Phys. 111 (1999) 5291.
[18] D. Kim, et al., Phys. Rev. B 67 (2003) 100406(R).
[19] D. Kim, et al., Phys. Rev. Lett. 89 (2002) 227202.
[20] D. Kim, et al., Phys. Rev. B 65 (2002) 214424.
[21] G.A. Jorge, et al., Phys. Rev. B 69 (2004) 174506.
[22] B.L. Zink, et al., Rev. Sci. Instrum. 73 (2002) 1841.
[23] B.L. Zink et, F. Hellman, Sol. St. Comm. 129 (2004) 199.
[24] B. Revaz, et al., Rev. Sci. Instrum. 74 (2003) 4389.
[25] Our Si-N films are prepared with similar recipes in the same furnace used in Mastangelo's study [26].
[26] C.H. Mastrangelo, Y.-C. Tai, R.S. Muller, Sens. Actuators A A23 (1990) 856.
[27] (a) A. Junod, in: A. Narlikar (Ed.), Studies of High Temperature Superconductors, vol. 19, Nova Science, Commack, New York, 1996, p. 1;
(b) Y. Wang, B. Revaz, A. Erb, A. Junod, Phys. Rev. B 63 (2001) 94508.
[28] The other two arms of the bridge are contained in a homemade computer controlled electronic system with variable resistors and capacitors and isolation transformers, which is described fully in a previous publication [1].
[29] R.J. Corruccini, J.J. Gniewek (Eds.), Specific Heats and Enthalpies of Technical Solids at Low Temperatures, 21, National Bureau of Standards Monograph, United States Departement of Commerce, Washington, DC, 1960.
[30] Y.S. Touloukian (Ed.), Specific Heat: Elements and Metallic Alloys, IFI/Plenum, New York, 1970.
[31] B.L. Zink, Ph.D. thesis, University of California at San Diego, 2002.
[32] R. Bachmann, et al., Rev. Sci. Instrum. 43 (1972) 205.
[33] B.L. Zink, B. Revaz, J.J. Cherry, F. Hellman, Rev. Sc. Instrum. 76 (2005) 24901.
[34] B.L. Zink, Ph.D. thesis, University of California at San Diego, 2002.
[35] R. Pietri, unpublished.
[36] K. Allen, Ph.D. thesis, University of California at San Diego, 1998.
[37] R.O. Pohl, X. Liu, E. Thompson, Rev. Mod. Phys. 74 (2002) 991.
[38] R.C. Zeller, R.O. Pohl, Phys. Rev. B 4 (1971).
[39] D.G. Cahill, R. Pohl, Ann. Rev. Phys. Chem. 39 (1988) 93.
[40] M.A. Ramos, U. Buchenau, in: P. Esquinazi (Ed.), Tunneling Systems in Amorphous and Crystalline Solids, Springer-Verlag, Berlin, 1998.
[41] X. Liu, H.v. Lohneysen, Europhys. Lett. 33 (1996) 617.
[42] I.Y. Guzman, A.F. Demidenko, V.I. Koshchenko, M.S. Fraifel'd, Y.V. Egner, Inorg. Mater. 12 (1976) 1546.
[43] W. Holmes, J.M. Gildemeister, P.L. Richards, V. Kotsubo, Appl. Phys. Lett. 72 (1998) 2250.
[44] S. Wenzel, Ph.D. thesis, University of California, Berkeley, 1992.
[45] S.T. Huxtable, unpublished.
[46] S.M. Lee, D.G. Cahill, J. Appl. Phys. 81 (1997) 2590.
[47] T. Klitsner, J.E. VanCleve, H.E. Fischer, R.O. Pohl, Phys. Rev. 38 (1988) 7576.